MATERIALS CHEMISTRY
FRONTIERS

RESEARCH ARTICLE

View Article Online
View Journal | View Issue

Cite this: *Mater. Chem. Front.*, 2022, **6**, 1310

Two-dimensional BA_2PbBr_4-based wafer for X-rays imaging application†

Youkui Xu,‡ Yingtao Li,‡ Qian Wang,* Huanyu Chen, Yutian Lei, Xuefeng Feng, Zhipeng Ci and Zhiwen Jin*

Received 15th March 2022,
Accepted 6th April 2022

DOI: 10.1039/d2qm00233g

rsc.li/frontiers-materials

As one of the most promising candidates for X-rays imaging materials, perovskites have received extensive attention. However, poor stability and undesirable ion migration are still obstacles to its development. In recent years, the successfully developed two-dimensional (2D) perovskite materials have skillfully solved the above-mentioned problems, but the preparation of their pure phase single crystals remains a great challenge. Here, a 2D perovskite single crystal, BA_2PbBr_4, was used as a representative model, which was grown *via* a simple synthesis method of the solution temperature lowering (STL), exhibiting a short fluorescence lifetime (6.82 ns), intense X-rays radioluminescence, and high environmental and temperature stability. Moreover, it has been used in X-rays imaging, which shows good imaging results and stability. This study demonstrates that 2D perovskites have great potential in low-cost X-rays imaging systems.

Introduction

Since X-rays were first discovered by Wilhelm Röntgen in 1895, the development of X-rays related technologies has brought great convenience to human life, such as medical diagnosis, non-destructive testing, substance identification, and safety inspection.[1–3] The basic principle of all these technologies is that X-rays interact with the material when the object is irradiated, and the emitted or reflected X-rays reflect object information. Therefore, the effective detection of X-rays with object information is particularly important, which is directly related to the performance of the instrument.[4,5]

Converting high-energy X-rays photons into visible light is one of the most common X-rays detection methods, namely, X-rays imaging.[6–12] At present, the successfully applied X-rays imaging materials include doped sodium iodide (NaI:Tl), doped cesium iodide (CsI:Tl), and oxide scintillator ($CdWO_4$, $Bi_4Ge_3O_{12}$).[13–16] However, they still have some drawbacks such as detectable energy range, high fabrication temperature, and poor stability. In recent years, due to their excellent photoluminescence quantum yield (PLQY), adjustable band gap, simple preparation process, and large atomic number (Z), halide perovskite materials have been widely used by researchers in the field of X-rays imaging and have achieved rapid development.[17–24] However, perovskites are of ionic crystals, which cause ion migration to occur easily under the radiation, temperature cycle, and electric field, therefore impacting the performance and stability of the device.[25,26]

Creatively, to overcome the unfavorable ion migration and poor stability, researchers introduced organic molecules into the perovskite structure to form a two-dimensional (2D) perovskite, in which lead halide octahedral sheets are separated by an organic spacer.[27–33] The organic spacer increases the activation energy of ion transport and therefore inhibits ion migration.[34,35] Furthermore, due to the steric hindrance produced by the organic spacer, it will increase the required for the phase transition to the non-perovskite phase, therefore improving the stability of the perovskite.[36]

Among many amine organic molecules, butylamine (BA), as a chain organic molecule, has been used as one of the most commonly used organic molecules in the preparation of 2D perovskites.[37] Sun *et al.* prepared BA-based 2D perovskites and discovered the ferroelectricity of 2D perovskites for the first time, and applied them in the field of photodetection.[38] Dravid *et al.* studied the mechanical properties of BA-based 2D perovskites.[39,40] Yang *et al.* prepared a blue LED (light-emitting diode) with high-color purity based on BA-based 2D perovskites.[41] Nevertheless, the size of the 2D perovskite single crystals prepared in the above work is in the order of hundreds of micrometers. Further, the introduction of organic molecules also makes it difficult to control the crystallization kinetics of the 2D perovskite.[42–47] Also, the as-prepared 2D perovskite is usually a multi-phase mixture, that is, 2D, quasi-2D, and 3D structures are mixed.[48–51] Therefore, one most troublesome

School of Physical Science and Technology & School of Materials and Energy & Key Laboratory for Magnetism and Magnetic Materials of MoE, Lanzhou University, Lanzhou 730000, China. E-mail: qianwang@lzu.edu.cn, jinzw@lzu.edu.cn

† Electronic supplementary information (ESI) available: Synthesis details, additional figures. See DOI: https://doi.org/10.1039/d2qm00233g

‡ These authors contributed equally to this work.

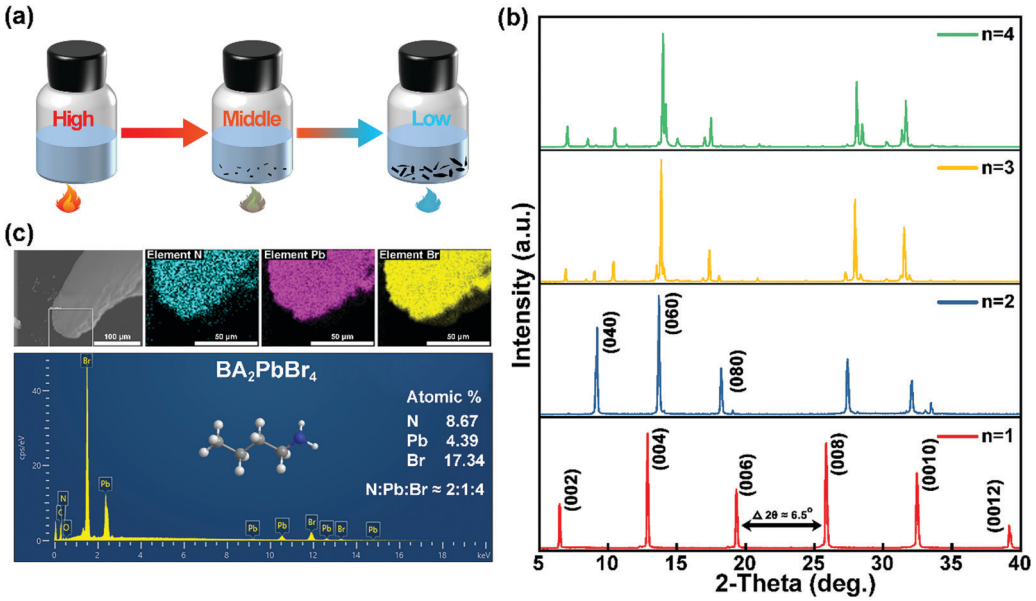

Fig. 1 Synthesis method and structure characterization of $BA_2MA_{n-1}Pb_nBr_{3n+1}$: (a) schematic of synthesis steps; (b) XRD; (c) elemental analysis of BA_2PbBr_4 (n = 1).

problem at present is the preparation of pure phase 2D perovskite.

In this study, we introduced a simple method of solution temperature lowering (STL) (perovskite precursor solution dissolves at higher temperature, and the solution reaches supersaturation and precipitates crystals when the temperature gradually decreases) to prepare a pure phase centimeter-scale 2D perovskite BA_2PbBr_4 and apply it to X-rays imaging. Further characterization suggests that the as-prepared 2D perovskite BA_2PbBr_4 is single crystal, has short fluorescence decay lifetime (6.82 ns), and exhibits excellent environmental and temperature stability. We believe that these results can inspire further research on the design of 2D perovskites for X-rays imaging.

Results and discussion

For the synthesis of 2D perovskite $BA_2MA_{n-1}Pb_nBr_{3n+1}$ (n = 1, 2, 3, 4), we adopted a simple method of STL.[52] As shown in Fig. 1(a), the precursor solvent is first dissolved at a high temperature (~100 °C) and then slowly cooled (1 °C min^{-1}); the solution reaches supersaturation and crystals are precipitated. The detailed experimental procedures are described in the (ESI†). Fig. 1(b) and Fig. S1 (ESI†) show the X-rays diffraction spectrum (XRD). Clearly, when n = 1, the diffraction peaks appear at equal intervals ($\Delta 2\theta \approx 6.5°$), which can be attributed to the same family of the crystal planes {001}. It implies that a 2D perovskite single crystal is formed. However, when n = 2, 3, 4 and higher n-values, the diffraction peaks of the sample are relatively mixed, which indicates that there are other n value 2D perovskites. In order to further verify the as-prepared 2D perovskite with n = 1 is a pure phase, elemental analysis was implemented. As shown in Fig. 1(c), the uniform distribution of the elements: nitrogen (N), lead (Pb), and bromine (Br) is shown. It is particularly worth noting that the atomic ratio of the three elements (N : Pb : Br) is close to 2 : 1 : 4, which is highly similar to the stoichiometric ratio in the chemical formula, further confirming that BA_2PbBr_4 is a pure phase 2D perovskite.

Fig. S1a (ESI†) is a scanning electron microscopy (SEM) picture of the 2D perovskite with different n values. When

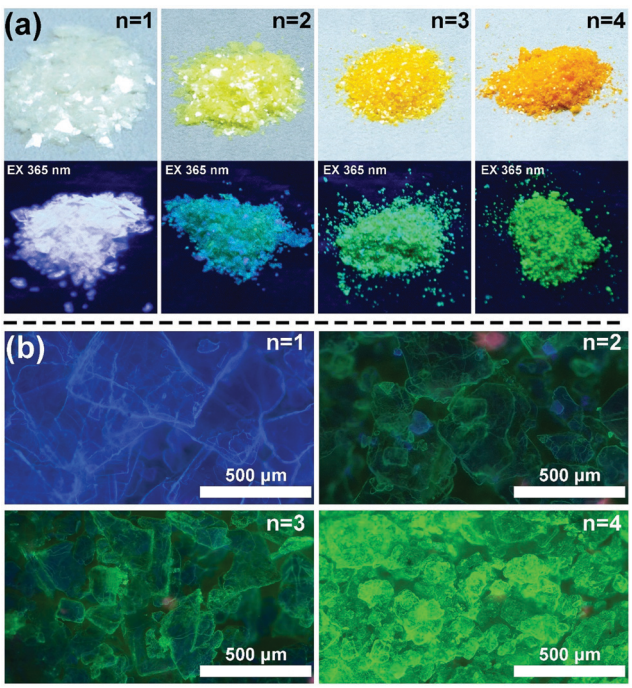

Fig. 2 Optical photos of $BA_2MA_{n-1}Pb_nBr_{3n+1}$: (a) digital photos of 2D perovskite crystals with different n values under background light and 365 nm ultraviolet light; (b) microscopy pictures of 2D perovskite crystals with different n values under 365 nm ultraviolet light irradiation.

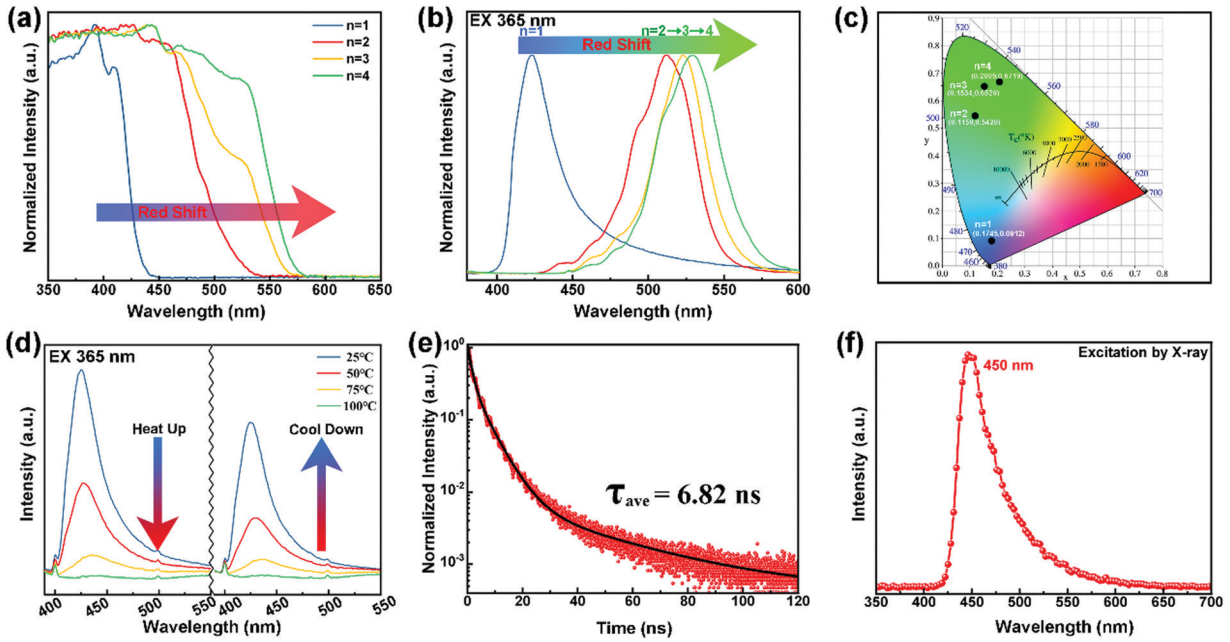

Fig. 3 $BA_2MA_{n-1}Pb_nBr_{3n+1}$ luminescence performance characterization: (a) UV-Vis absorption spectrum (UV-Vis); (b) photoluminescence spectrum (PL); (c) CIE chromaticity diagram; (d) BA_2PbBr_4 PL spectrum at different temperatures; (e) TRPL; (f) radioluminescence spectrum (RL).

n = 1, the 2D perovskite appears as a single large-scale sheet structure. With the n value increases, the morphology becomes disordered, showing a mixture of sheets with different sizes. This is mutually corroborated by the XRD results, that is, n = 1 is a pure phase 2D perovskite, while others are not. When n = 2, 3, and 4, the element analysis results are shown in Fig. S2b–d (ESI†), respectively. These three elements of N, Pb, and Br are uniformly distributed, implying the formation of the 2D perovskite, yet they are mixed phase. Further, in order to characterize the mechanical properties of 2D perovskites, we performed nanoindentation characterization of the 2D perovskite wafer with different n values (Fig. S3a, ESI†). Fig. S3b (ESI†) shows the trends of Young' modulus and hardness as a function of n for the 2D perovskite wafer. As the value of n increases, Young' modulus and hardness show the same trend and both increase, which is consistent with previous literature reports.[39,40,53]

Fig. 2(a) shows the digital photos of the as-synthesized 2D perovskites with different n values under background light and 365 nm ultraviolet. Under the background light, the 2D perovskite with n = 1 is a large sheet, the size of n = 2 is clearly reduced, and when n = 3, 4, it becomes fine granular, which is consistent with the results of SEM. Under the excitation of 365 nm ultraviolet light, as the n value increases, the emission color shifts from blue to green. The difference in the luminescence color of 2D perovskites with different n values is caused by the quantum confinement effect.[54–57] Fig. 2(b) is a microscopy picture of 2D perovskites with different n values under an optical microscope and excited with 365 nm ultraviolet light. When n = 1, it is pure blue light, and the others are a mixture of multiple colors, which further reveals that the 2D perovskites are a mixture of different n values.

In order to quantitatively characterize the luminescence properties of 2D perovskites with different n values, ultraviolet-visible absorption spectroscopy (UV-Vis) and photoluminescence spectroscopy (PL) were implemented (Fig. 3(a), (b), and Fig. S4, ESI†). Clearly, as n increases, both the absorption band edge and the PL emission peak position have evident red-shifts (CIE coordinates shown in Fig. 3(c)). Multiple exciton absorption peaks and shoulder emission peaks appear, which are caused by the mixing of impure phases. Fig. 3(d) shows the photoluminescence (PL) spectrum of BA_2PbBr_4 as a function of temperature. When the room temperature is gradually increased to 100 °C, the PL intensity gradually weakens to completely disappear, which is due to the serious tilt of the $[PbBr_6]^{4-}$ octahedron and the serious disorder of the organic chain caused by the increase in temperature, resulting in the reduction of the band gap.[41] However, it is worth noting that as the temperature gradually cools down to room temperature, the PL intensity gradually recovers, which indicates no occurrence of serious ion migration and collapses of the 2D perovskite crystal structure. Fig. 3(e) shows the time-resolved photoluminescence (TRPL) spectrum of BA_2PbBr_4. The decay curve was fitted with a three-exponential function, and the corresponding parameters are listed in Table S1 in the ESI,† and the calculation fluorescence lifetime is 6.82 ns. To characterize the luminescence performance of BA_2PbBr_4 under X-rays irradiation, radioluminescence spectroscopy (RL) was applied (Fig. 3(f)). There is an evident single emission peak at about 450 nm, implying the good luminescence performance under X-rays excitation.

All the above-mentioned characterization and analyses strongly proved that when n = 1, that is, BA_2PbBr_4 is a pure phase single crystal 2D perovskite, which has greater potential

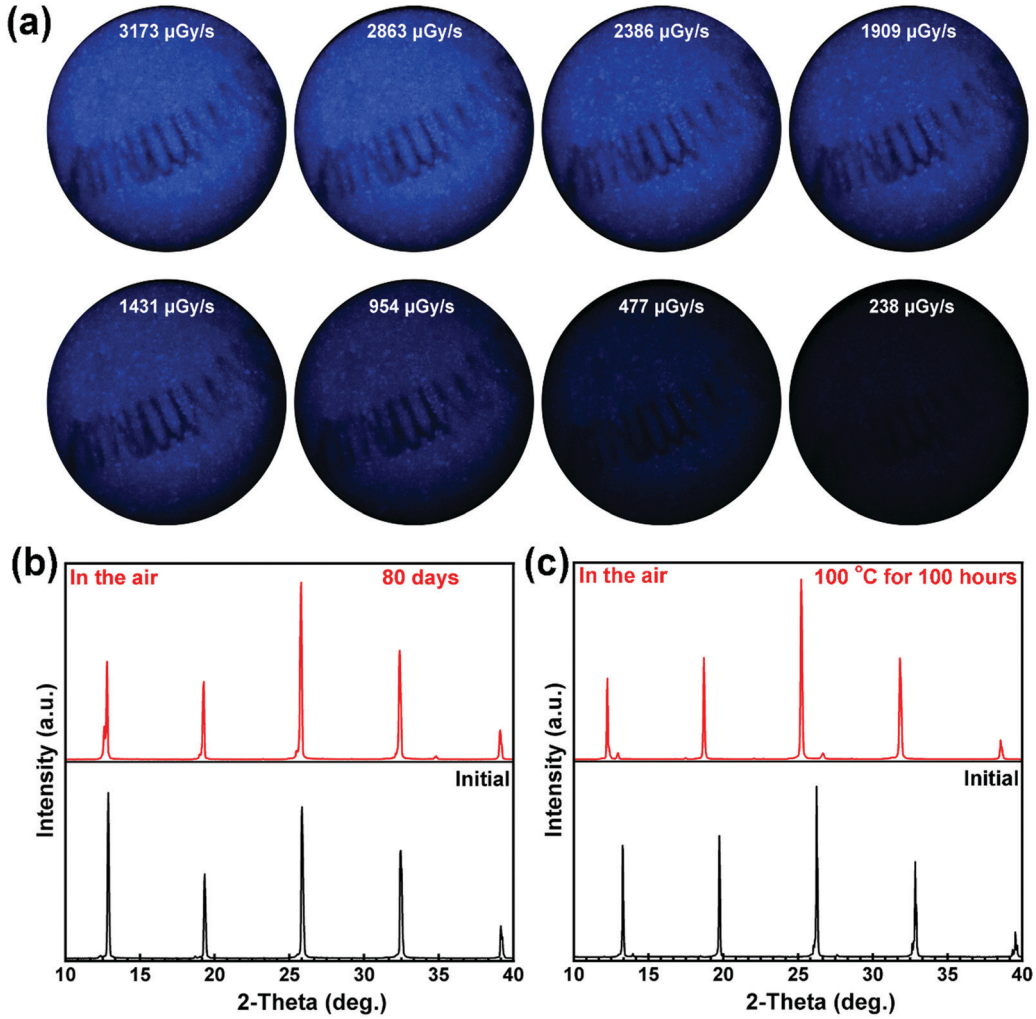

Fig. 4 X-rays imaging application and stability characterization: (a) imaging photos of the BA_2PbBr_4 wafer at different radiation dose rates; (b) XRD comparison of BA_2PbBr_4 before and after storage in the environment for 80 days; (c) XRD comparison of BA_2PbBr_4 before and after storage at 100 °C for 100 h.

in the X-rays imaging field than other impure phase samples. Based on this, we applied BA_2PbBr_4 in the field of X-rays imaging. Fig. 4(a) is the photograph of wafer BA_2PbBr_4 under different X-rays radiation rates, showing a clear outline of the object (spring), implying its potential as an X-rays scintillator imaging material. Further, its stability was also been considered. Fig. 4(b) shows the XRD comparison of BA_2PbBr_4 before and after being stored in the air for 80 days, and it does not show any signs of material degradation. Fig. 4(c) is a characterization of temperature stability. The XRD comparison of BA_2PbBr_4 before and after 100 h of storage in an air environment at 100 °C shows the corresponding peak positions with consistent deviation to a small angle, which may be due to the high temperature that weakened the coupling between organic–inorganic layers and increased the distance between adjacent inorganic octahedral. However, there is also no obvious sign of material degradation. Therefore, it can be considered that BA_2PbBr_4 has good environmental and temperature stability.

Conclusion

In conclusion, this study adopts the STL method to prepare a 2D perovskite pure phase single crystal (BA_2PbBr_4) for X-rays imaging. It exhibits intense radioluminescence with ultrafast fluorescence lifetime and makes it highly promising for instantaneous X-rays imaging with no significant afterglow interference. In addition, BA_2PbBr_4 exhibits excellent environmental and temperature stability. After 80 days and 100 °C for 100 h of storage in the environment without any protection, there is no sign of degradation. These findings demonstrate the potential of a 2D perovskite single crystal for promising low-cost X-rays imaging, including medical diagnostics, non-destructive testing, and safety inspection in the future.

Conflicts of interest

The authors declare no competing financial interests.

Acknowledgements

This work was funded by the National Natural Science Foundation of China (52073131, 51902148, and 51801088), the Fundamental Research Funds for the Central Universities (lzujbky-2021-59, lzujbky-2021-ct15, lzujbky-2021-ct01, and lzujbky-2021-sp69). The calculation work was supported by Supercomputing Center of Lanzhou University.

References

1 W. C. Röntgen, On a New Kind of Rays, *Science*, 1896, **3**, 227–231.
2 Y. C. Kim, K. H. Kim, D.-Y. Son, D.-N. Jeong, J.-Y. Seo, Y. S. Choi, I. T. Han, S. Y. Lee and N.-G. Park, Printable organometallic perovskite enables large-area, low-dose X-ray imaging, *Nature*, 2017, **550**, 87–91.
3 X. Xu, W. Qian, S. Xiao, J. Wang, S. Zheng and S. Yang, Halide perovskites: A dark horse for direct X-ray imaging, *EcoMat*, 2020, **2**, 12064.
4 Y. Zhou, J. Chen, O. M. Bakr and O. F. Mohammed, Metal halide perovskites for X-ray imaging scintillators and detectors, *ACS Energy Lett.*, 2021, **6**, 739–768.
5 W.-F. Wang, J. Lu, X.-M. Xu, B.-Y. Li, J. Gao, M.-J. Xie, S.-H. Wang, F.-K. Zheng and G.-C. Guo, Sensitive X-ray detection and imaging by a scintillating lead(II)-based metal–organic framework, *Chem. Eng. J.*, 2022, **430**, 133010.
6 W. Heiss and C. Brabec, Perovskites target X-ray detection, *Nat. Photonics*, 2016, **10**, 288–289.
7 F. Zhou, Z. Li, W. Lan, Q. Wang, L. Ding and Z. Jin, Halide perovskite, a potential scintillator for X-ray detection, *Small Methods*, 2020, **4**, 2000506.
8 P. Büchele, M. Richter, S. F. Tedde, G. J. Matt, G. N. Ankah, R. Fischer, M. Biele, W. Metzger, S. Lilliu, O. Bikondoa, J. E. Macdonald, C. J. Brabec, T. Kraus, U. Lemmer and O. Schmidt, X-ray imaging with scintillator-sensitized hybrid organic photodetectors, *Nat. Photonics*, 2015, **9**, 843–848.
9 X. Zhao, T. Jin, W. Gao, G. Niu, J. Zhu, B. Song, J. Luo, W. Pan, H. Wu, M. Zhang, X. He, L. Fu, Z. Li, H. Zhao and J. Tang, Embedding $Cs_3Cu_2I_5$ Scintillators into anodic aluminum oxide matrix for high-resolution X-ray imaging, *Adv. Opt. Mater.*, 2021, **9**, 2101194.
10 H. Li, H. Yang, R. Yuan, Z. Sun, Y. Yang, J. Zhao, Q. Li and Z. Zhang, Ultrahigh spatial resolution, fast decay, and stable X-ray scintillation screen through assembling $CsPbBr_3$ nanocrystals arrays in anodized aluminum oxide, *Adv. Opt. Mater.*, 2021, **9**, 2101297.
11 Z. Fang, H. Tang, Z. Yang, H. Zhang, Q. Peng, X. Yu, D. Zhou, J. Qiu and X. Xu, Transparent medium embedded with CdS quantum dots for X-ray imaging, *Adv. Opt. Mater.*, 2021, **9**, 2101607.
12 Q. He, C. Zhou, L. Xu, S. Lee, X. Lin, J. Neu, M. Worku, M. Chaaban and B. Ma, Highly stable organic antimony halide crystals for X-ray scintillation, *ACS Mater. Lett.*, 2020, **2**, 633–638.
13 S. Shrestha, R. Fischer, G. J. Matt, P. Feldner, T. Michel, A. Osvet, I. Levchuk, B. Merle, S. Golkar, H. Chen, S. F. Tedde, O. Schmidt, R. Hock, M. Rührig, M. Göken, W. Heiss, G. Anton and C. J. Brabec, High-performance direct conversion X-ray detectors based on sintered hybrid lead triiodide perovskite wafers, *Nat. Photonics*, 2017, **11**, 436–440.
14 H. Wei and J. Huang, Halide lead perovskites for ionizing radiation detection, *Nat. Commun.*, 2019, **10**, 1066.
15 M. Chen, L. Sun, X. Ou, H. Yang, X. Liu, H. Dong, W. Hu and X. Duan, Organic semiconductor single crystals for X-ray imaging, *Adv. Mater.*, 2021, **33**, 2104749.
16 H. Zhang, Z. Yang, M. Zhou, L. Zhao, T. Jiang, H. Yang, X. Yu, J. Qiu, Y. Yang and X. Xu, Reproducible X-ray imaging with a perovskite nanocrystal scintillator embedded in a transparent amorphous network structure, *Adv. Mater.*, 2021, **33**, 2102529.
17 W. Wei, Y. Zhang, Q. Xu, H. Wei, Y. Fang, Q. Wang, Y. Deng, T. Li, A. Gruverman, L. Cao and J. Huang, Monolithic integration of hybrid perovskite single crystals with heterogenous substrate for highly sensitive X-ray imaging, *Nat. Photonics*, 2017, **11**, 315–321.
18 H. Tsai, F. Liu, S. Shrestha, K. Fernando, S. Tretiak, B. Scott, D. T. Vo, J. Strzalka and W. Nie, A sensitive and robust thin-film x-ray detector using 2D layered perovskite diodes, *Sci. Adv.*, 2020, **6**, eaay0815.
19 Y. Liu, Z. Xu, Z. Yang, Y. Zhang, J. Cui, Y. He, H. Ye, K. Zhao, H. Sun, R. Lu, M. Liu, M. G. Kanatzidis and S. Liu, Inch-size 0D-Structured lead-free perovskite single crystals for highly sensitive stable X-ray imaging, *Matter*, 2020, **3**, 180–196.
20 L. Yang, H. Zhang, M. Zhou, L. Zhao, W. Chen, T. Wang, X. Yu, D. Zhou, J. Qiu and X. Xu, High-stable X-ray imaging from all-inorganic perovskite nanocrystals under a high dose radiation, *J. Phys. Chem. Lett.*, 2020, **11**, 9203–9209.
21 X. Ou, X. Qin, B. Huang, J. Zan, Q. Wu, Z. Hong, L. Xie, H. Bian, Z. Yi, X. Chen, Y. Wu, X. Song, J. Li, Q. Chen, H. Yang and X. Liu, High-resolution X-ray luminescence extension imaging, *Nature*, 2021, **590**, 410–415.
22 W. Ma, T. Jiang, Z. Yang, H. Zhang, Y. Su, Z. Chen, X. Chen, Y. Ma, W. Zhu, X. Yu, H. Zhu, J. Qiu, X. Liu, X. Xu and Y. Yang, Highly resolved and robust dynamic X-Ray imaging using perovskite glass-ceramic scintillator with reduced light scattering, *Adv. Sci.*, 2021, **8**, 2003728.
23 D. Shi, V. Adinolfi, R. Comin, M. Yuan, E. Alarousu, A. Buin, Y. Chen, S. Hoogland, A. Rothenberger, K. Katsiev, Y. Losovyj, X. Zhang, P. A. Dowben, O. F. Mohammed, E. H. Sargent and O. M. Bakr, Low trap-state density and long carrier diffusion in organolead trihalide perovskite single crystals, *Science*, 2015, **347**, 519.
24 Y. Liu, Z. Yang and S. Liu, Recent progress in single-crystalline perovskite research including crystal preparation, property evaluation, and applications, *Adv. Sci.*, 2018, **5**, 1700471.
25 P. V. Kamat and M. Kuno, Halide ion migration in perovskite nanocrystals and nanostructures, *Acc. Chem. Res.*, 2021, **54**, 520–531.
26 Z. Li, F. Zhou, H. Yao, Z. Ci, Z. Yang and Z. Jin, Halide perovskites for high-performance X-ray detector, *Mater. Today*, 2021, **48**, 155–175.

27 H. Li, J. Song, W. Pan, D. Xu, W.-a. Zhu, H. Wei and B. Yang, Sensitive and stable 2D perovskite single-crystal X-ray detectors enabled by a supramolecular anchor, *Adv. Mater.*, 2020, **32**, 2003790.

28 Y. Fu, X. Jiang, X. Li, B. Traore, I. Spanopoulos, C. Katan, J. Even, M. G. Kanatzidis and E. Harel, Cation engineering in two-dimensional Ruddlesden–Popper lead iodide perovskites with mixed large a-site cations in the cages, *J. Am. Chem. Soc.*, 2020, **142**, 4008–4021.

29 J. Zhao, Y. Zhao, Y. Guo, X. Zhan, J. Feng, Y. Geng, M. Yuan, X. Fan, H. Gao, L. Jiang, Y. Yan and Y. Wu, Layered metal-halide perovskite single-crystalline microwire arrays for anisotropic nonlinear optics, *Adv. Funct. Mater.*, 2021, **31**, 2105855.

30 J. Euvrard, Y. Yan and D. B. Mitzi, Electrical doping in halide perovskites, *Nat. Rev. Mater.*, 2021, **6**, 531–549.

31 T. Li, X. Chen, X. Wang, H. Lu, Y. Yan, M. C. Beard and D. B. Mitzi, Origin of broad-band emission and impact of structural dimensionality in tin-alloyed Ruddlesden–Popper hybrid lead iodide perovskites, *ACS Energy Lett.*, 2020, **5**, 347–352.

32 M. K. Jana, S. M. Janke, D. J. Dirkes, S. Dovletgeldi, C. Liu, X. Qin, K. Gundogdu, W. You, V. Blum and D. B. Mitzi, Direct-Bandgap 2D Silver–Bismuth Iodide Double Perovskite: The Structure-Directing Influence of an Oligothiophene Spacer Cation, *J. Am. Chem. Soc.*, 2019, **141**, 7955–7964.

33 Y. Liang, K. J. Manoj, C. S. Peter, B. M. David and Y. Wei, Alkyl–Aryl Cation Mixing in Chiral 2D Perovskites, *J. Am. Chem. Soc.*, 2021, **143**, 18114–18120.

34 X. Xiao, J. Dai, Y. Fang, J. Zhao, X. Zheng, S. Tang, P. N. Rudd, X. C. Zeng and J. Huang, Suppressed Ion Migration along the In-Plane Direction in Layered Perovskites, *ACS Energy Lett.*, 2018, **3**, 684–688.

35 Y. Lin, Y. Bai, Y. Fang, Q. Wang, Y. Deng and J. Huang, Suppressed Ion Migration in Low-Dimensional Perovskites, *ACS Energy Lett.*, 2017, **2**, 1571–1572.

36 Y. Shao, W. Gao, H. Yan, R. Li, I. Abdelwahab, X. Chi, L. Rogée, L. Zhuang, W. Fu, S. P. Lau, S. F. Yu, Y. Cai, K. P. Loh and K. Leng, Unlocking surface octahedral tilt in two-dimensional Ruddlesden–Popper perovskites, *Nat. Commun.*, 2022, **13**, 138.

37 M. D. Smith, A. Jaffe, E. R. Dohner, A. M. Lindenberg and H. I. Karunadasa, Structural origins of broadband emission from layered Pb–Br hybrid perovskites, *Chem. Sci.*, 2017, **8**, 4497–4504.

38 L. Li, Z. Sun, P. Wang, W. Hu, S. Wang, C. Ji, M. Hong and J. Luo, Tailored engineering of an unusual $(C_4H_9NH_3)_2(CH_3NH_3)_2Pb_3Br_{10}$ two-dimensional multilayered perovskite ferroelectric for a high-performance photodetector, *Angew. Chem., Int. Ed.*, 2017, **56**, 12150–12154.

39 Q. Tu, I. Spanopoulos, S. Hao, C. Wolverton, M. G. Kanatzidis, G. S. Shekhawat and V. P. Dravid, Out-of-plane mechanical properties of 2D hybrid organic–inorganic perovskites by nanoindentation, *ACS Appl. Mater. Interfaces*, 2018, **10**, 22167–22173.

40 Q. Tu, I. Spanopoulos, E. S. Vasileiadou, X. Li, M. G. Kanatzidis, G. S. Shekhawat and V. P. Dravid, Exploring the factors affecting the mechanical properties of 2D hybrid organic–inorganic perovskites, *ACS Appl. Mater. Interfaces*, 2020, **12**, 20440–20447.

41 H. Chen, J. Lin, J. Kang, Q. Kong, D. Lu, J. Kang, M. Lai, N. Quan Li, Z. Lin, J. Jin, L.-w. Wang, F. Toney Michael and P. Yang, Structural and spectral dynamics of single-crystalline Ruddlesden–Popper phase halide perovskite blue light-emitting diodes, *Sci. Adv.*, 2020, **6**, eaay4045.

42 X. Youkui, W. Meng, L. Yutian, C. Zhipeng and J. Zhiwen, Crystallization kinetics in 2D perovskite solar cells, *Adv. Energy Mater.*, 2020, **10**, 2002558.

43 X. Zhao, T. Liu and Y.-L. Loo, Advancing 2D perovskites for efficient and stable solar cells: Challenges and opportunities, *Adv. Mater.*, 2021, **33**, 2105849.

44 Z. Guo, Y. Zhang, B. Wang, L. Wang, N. Zhou, Z. Qiu, N. Li, Y. Chen, C. Zhu, H. Xie, T. Song, L. Song, H. Xue, S. Tao, Q. Chen, G. Xing, L. Xiao, Z. Liu and H. Zhou, Promoting energy transfer via manipulation of crystallization kinetics of quasi-2D perovskites for efficient green light-emitting diodes, *Adv. Mater.*, 2021, **33**, 2102246.

45 J. Guo, Z. Shi, J. Xia, K. Wang, Q. Wei, C. Liang, D. Zhao, Z. Zhang, S. Chen, T. Liu, S. Mei, W. Hui, G. Hong, Y. Chen and G. Xing, Phase tailoring of Ruddlesden–Popper perovskite at fixed large spacer cation ratio, *Small*, 2021, **17**, 2100560.

46 Y. Gao, E. Shi, S. Deng, S. B. Shiring, J. M. Snaider, C. Liang, B. Yuan, R. Song, S. M. Janke, A. Liebman-Peláez, P. Yoo, M. Zeller, B. W. Boudouris, P. Liao, C. Zhu, V. Blum, Y. Yu, B. M. Savoie, L. Huang and L. Dou, Molecular engineering of organic-inorganic hybrid perovskites quantum wells, *Nat. Chem.*, 2019, **11**, 1151–1157.

47 J. Song, G. Zhou, W. Chen, Q. Zhang, J. Ali, Q. Hu, J. Wang, C. Wang, W. Feng, A. B. Djurišić, H. Zhu, Y. Zhang, T. Russell and F. Liu, Unraveling the crystallization kinetics of 2D perovskites with sandwich-type structure for high-performance photovoltaics, *Adv. Mater.*, 2020, **32**, 2002784.

48 C. Liang, H. Gu, Y. Xia, Z. Wang, X. Liu, J. Xia, S. Zuo, Y. Hu, X. Gao, W. Hui, L. Chao, T. Niu, M. Fang, H. Lu, H. Dong, H. Yu, S. Chen, X. Ran, L. Song, B. Li, J. Zhang, Y. Peng, G. Shao, J. Wang, Y. Chen, G. Xing and W. Huang, Two-dimensional Ruddlesden–Popper layered perovskite solar cells based on phase-pure thin films, *Nat. Energy*, 2020, **6**, 38–45.

49 C. M. M. Soe, G. P. Nagabhushana, R. Shivaramaiah, H. Tsai, W. Nie, J.-C. Blancon, F. Melkonyan, D. H. Cao, B. Traoré, L. Pedesseau, M. Kepenekian, C. Katan, J. Even, T. J. Marks, A. Navrotsky, A. D. Mohite, C. C. Stoumpos and M. G. Kanatzidis, Structural and thermodynamic limits of layer thickness in 2D halide perovskites, *Proc. Natl. Acad. Sci. U. S. A.*, 2019, **116**, 58–66.

50 R. J. E. Westbrook, W. Xu, X. Liang, T. Webb, T. M. Clarke and S. A. Haque, 2D phase purity determines charge-transfer yield at 3D/2D lead halide perovskite heterojunctions, *J. Phys. Chem. Lett.*, 2021, **12**, 3312–3320.

51 S. Sidhik, W. Li, M. H. K. Samani, H. Zhang, Y. Wang, J. Hoffman, A. K. Fehr, M. S. Wong, C. Katan, J. Even, A. B. Marciel, M. G. Kanatzidis, J.-C. Blancon and A. D. Mohite, Memory seeds enable high structural phase

purity in 2D perovskite films for high-efficiency devices, *Adv. Mater.*, 2021, **33**, 2007176.

52 F. Liu, L. Wang, J. Wang, F. Wang, Y. Chen, S. Zhang, H. Sun, J. Liu, G. Wang, Y. Hu and C. Jiang, 2D Ruddlesden–Popper perovskite single crystal field-effect transistors, *Adv. Funct. Mater.*, 2020, **31**, 2005662.

53 M. Kepenekian, B. Traore, J.-C. Blancon, L. Pedesseau, H. Tsai, W. Nie, C. C. Stoumpos, M. G. Kanatzidis, J. Even, A. D. Mohite, S. Tretiak and C. Katan, Concept of lattice mismatch and emergence of surface states in two-dimensional hybrid perovskite quantum wells, *Nano Lett.*, 2018, **18**, 5603–5609.

54 D. H. Cao, C. C. Stoumpos, O. K. Farha, J. T. Hupp and M. G. Kanatzidis, 2D Homologous perovskites as light-absorbing materials for solar cell applications, *J. Am. Chem. Soc.*, 2015, **137**, 7843–7850.

55 L. Mao, W. Ke, L. Pedesseau, Y. Wu, C. Katan, J. Even, M. R. Wasielewski, C. C. Stoumpos and M. G. Kanatzidis, Hybrid Dion-Jacobson 2D lead iodide perovskites, *J. Am. Chem. Soc.*, 2018, **140**, 3775–3783.

56 B. Cai, X. Li, Y. Gu, M. Harb, J. Li, M. Xie, F. Cao, J. Song, S. Zhang, L. Cavallo and H. Zeng, Quantum confinement effect of two-dimensional all-inorganic halide perovskites, *Sci. China Mater.*, 2017, **60**, 811–818.

57 X. Li, J. M. Hoffman and M. G. Kanatzidis, The 2D halide perovskite rulebook: How the spacer influences everything from the structure to optoelectronic device efficiency, *Chem. Rev.*, 2021, **121**, 2230–2291.

